Journal of Energy Storage 86 (2024) 111310

Contents lists available at ScienceDirect

Journal of Energy Storage

journal homepage: www.elsevier.com/locate/est

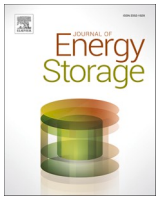

Research Papers

Sodium acetate-based thermochemical energy storage with low charging temperature and enhanced power density

Juan Arcenegui-Troya [a,*], Jesus Lizana [b], Pedro Enrique Sánchez-Jiménez [c,d,**], Antonio Perejón [c,d,**], Andrea Vañes-Vallejo [c], Luis Allan Pérez-Maqueda [c,*]

[a] Department of Engineering, Universidad Loyola Andalucía, Avda. de las Universidades s/n, 41704 Dos Hermanas, Seville, Spain
[b] Department of Engineering Science, Oxford University, Parks Road, Oxford, OX1 3PJ, United Kingdom
[c] Instituto de Ciencia de Materiales de Sevilla, C. S. I. C.-Universidad de Sevilla, C. Américo Vespucio nº 49, 41092 Sevilla, Spain
[d] Departamento de Química Inorgánica, Facultad de Química, Universidad de Sevilla, 41012 Sevilla, Spain

ARTICLE INFO

Keywords:
Salt hydrate
Sodium acetate
Hydration
Heating
Thermal energy storage
Thermochemical storage
Net-zero energy buildings

ABSTRACT

The electrification of heat necessitates the development of innovative domestic heat batteries to effectively balance energy demand with renewable power supply. Thermochemical heat storage systems show great promise in supporting the electrification of heating, thanks to their high thermal energy storage density and minimal thermal losses. Among these systems, salt hydrate-based thermochemical systems are particularly appealing. However, they do suffer from slow hydration kinetics in the presence of steam, which limits the achievable power density. Additionally, their relatively high dehydration temperature hinders their application in supporting heating systems. Furthermore, there are still challenges regarding the appropriate thermodynamic, physical, kinetic, chemical, and economic requirements for implementing these systems in heating applications. This study analyzes a proposal for thermochemical energy storage based on the direct hydration of sodium acetate with liquid water. The proposed scheme satisfies numerous requirements for heating applications. By directly adding liquid water to the salt, an unprecedented power density of 5.96 W/g is achieved, nearly two orders of magnitude higher than previously reported for other salt-based systems that utilize steam. Albeit the reactivity drops as a consequence of deliquescence and particle aggregation, it has been shown that this deactivation can be effectively mitigated by incorporating 10 % silica, achieving lower but stable energy and power density values. Furthermore, unlike other salts studied previously, sodium acetate can be fully dehydrated at temperatures within the ideal range for electrified heating systems such as heat pumps (40 °C – 60 °C). The performance of the proposed scheme in terms of dehydration, hydration, and multicyclic behavior is determined through experimental analysis.

1. Introduction

Reducing dependency on fossil fuels in the energy sector requires the complete decarbonisation of heating, which currently accounts for over 20 % of global energy consumption [1]. Electrifying heat generation has emerged as the most promising solution for achieving decarbonisation [2]. However, the electrification of heating with low-carbon technologies requires the development of innovative and flexible energy solutions to address the substancial increase in peak power demand and the mismatch between renewable power supply and demand [3,4].

A promising approach towards achieving a low-carbon heating sector involves energy-efficient buildings equipped with thermal energy storage (TES) solutions integrated into efficient electric heating systems, such as heat pumps (HPs), to reduce and balance power demand [2]. This has sparked a search for advanced TES systems that operate at temperatures suitable for heating purposes [5–7]. Among the proposed TES systems, which include sensible [8], latent [9] and thermochemical energy storage (TCES), the latter stands out due to its potential for high energy densities and long-term energy storage with minimal thermal losses [10,11].

* Corresponding authors.
** Corresponding authors at: Instituto de Ciencia de Materiales de Sevilla, C. S. I. C.-Universidad de Sevilla, C. Américo Vespucio nº 49, 41092 Sevilla, Spain.
E-mail addresses: jjarcenegui@icmse.csic.es (J. Arcenegui-Troya), pedro.enrique@icmse.csic.es (P.E. Sánchez-Jiménez), aperejon@us.es (A. Perejón), maqueda@icmse.csic.es (L.A. Pérez-Maqueda).

https://doi.org/10.1016/j.est.2024.111310
Received 27 October 2023; Received in revised form 15 January 2024; Accepted 10 March 2024
Available online 23 March 2024

Salt hydrates have garnered significant interest as thermochemical materials (TCMs) due to their properties that make them suitable for low to medium-temperature applications [12–15]. In the charging process, renewable energy sources can drive the endothermic dehydration of salt hydrates-based TCES (SH-TCES). The resulting anhydrous salt is then stored to produce exothermic hydration when required [16].

Several single salt hydrates have been investigated for TCES due to their high thermal energy storage density (TESD), including $MgSO_4{\cdot}7H_2O$ [17], $MgCl_2{\cdot}6H_2O$ [18] $KCO_3{\cdot}1.5H_2O$ [19] $Na_2S{\cdot}5H_2O$ [20] and $SrBr_2{\cdot}6H_2O$ [21]. Fig. 1 illustrates the theoretical values of TESD as a function of dehydration temperature for some salts proposed for SH-TCES in low-temperature applications (< 130 °C). The lowest and highest hydrates involved are indicated in parentheses, with an arrow indicating the direction of the reaction (hydration). The values of TESD were obtained from Donkers et al.'s review on salt hydrates for domestic heating applications [12].

As shown, most of the previously studied salt hydrates exhibit dehydration (charging) temperatures between 80 °C and 150 °C [25–27], which is too high for heating applications in buildings [16]. Ideally, heating applications require operating temperatures during charging and discharging cycles between 40 °C and 60 °C, which are suitable for most common domestic heat technologies [28,29]. Fig. 1 demonstrates that only two salts have charging temperatures within the ideal range (highlighted in cyan) for domestic heating applications [29]. However, these salts ($CuCl_2$ and $FeCl_2$) have been discarded due to their high cost and chemical instability [12]. Other disadvantages shared by many studied salts include poor and very slow re-hydration capability (such as in the cases of $MgSO_4$ and $FeCl_2$), corrosiveness issues (such as in the case of Na_2S) and high price (such as in the cases of $SrBr_2{\cdot}6H_2O$ and $CuCl_2$) [12,16]. An effective strategy to overcome these limitations involves using inert materials as supporting matrices with high porosity [30]. For example, zeolite matrices have been demonstrated to improve the thermal stability and the multicycle performance of $MgSO_4$ [31–33]. Expanded vermiculite matrices have been utilized as supports for $SrBr_2$ and K_2CO_3, showcasing their ability to prevent leakage and corrosiveness by retaining the solution formed after deliquescence within the macropores of the matrix [34–36]. Carbon-based materials, such as natural graphite, typically exhibit high specific surface area and porosity, along with large thermal conductivity values. These characteristics are advantageous for confining salt powder and enhancing heat and mass transfer, making them attractive candidates for matrices [37,38]. Metal-organic frameworks (MOFs) are also utilized as inert materials for supporting matrices. The results obtained with $CaCl_2$-coated MOFs elucidate that these composites, containing hydrophilic groups, exhibit an enhanced moisture adsorption capacity compared to pure $CaCl_2$. Additionally, they demonstrate satisfying cyclability [39,40]. However, the use of inert materials as supports entails a significant reduction in TESD [41].

The power density (PD) is a critical factor to consider when evaluating the viability of using a salt hydrate for heating applications. It is defined as the ratio between TESD and the time required to achieve the maximum conversion value, estimated from the evolution of the hydration time as depicted in the cited works [12]. The PD should align with the peak capacity of the heating system (heat pump or boiler) necessary for the specific application. In residential settings, the peak capacity of heating systems can range from 4 kW to 12 kW, depending on the type of housing [42]. This peak capacity ensures that the heating system can adequately warm the indoor environment to meet thermal comfort requirements during the coldest hours and days. Therefore, the thermal discharge capacity of the SH-TCES system should match or come close to this peak capacity in order to satisfy indoor thermal comfort requirements. Insufficient heat release capacity from the TES unit will hinder achieving the desired set-point temperature [42]. As observed in Fig. 1b, the PD of the studied SH-TCES systems thus far is approximately 0.1 W/g, which necessitates the use of at least 40 kg of TCM to meet the heating application requirements. The PD is directly influenced by the kinetics of hydration and dehydration, with the reaction speed playing a significant role in the design of reactors and operating conditions in SH-TCES [15,43–45].

Hence, achieving low dehydration temperatures and high power densities remains a crucial objective in the quest for efficient SH-TCES systems. This creates opportunities to investigate new conditions and materials that meet the necessary criteria for implementing this technology on a large scale. Alternative approaches for SH-TCES, such as those based on hydration via liquid water, can enhance hydration kinetics and consequently increase the PD, leading to a significant reduction in the required amount of TCM. Furthermore, gas (steam)-solid reactions often involve different tanks and heat exchangers,

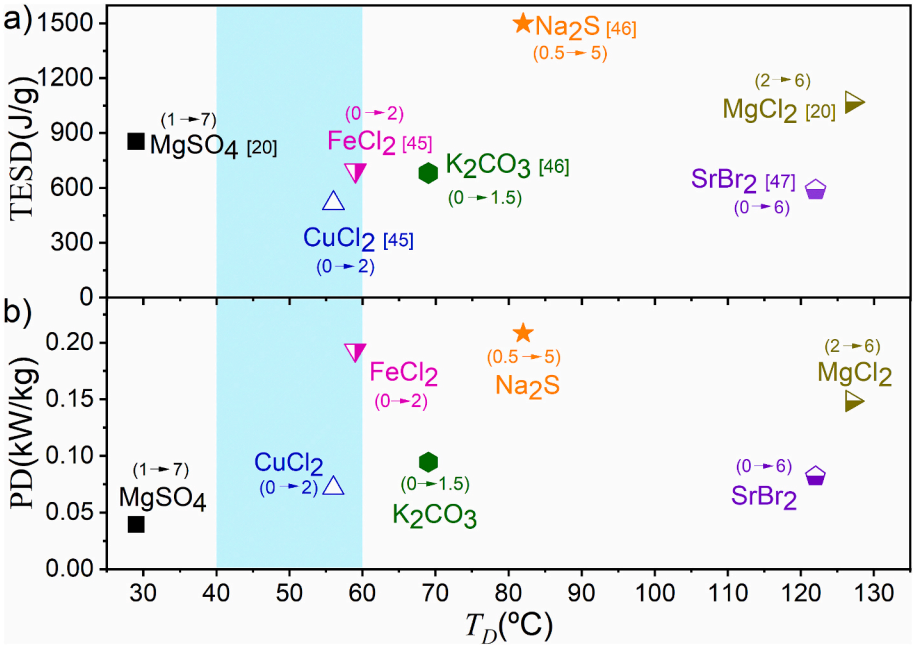

Fig. 1. a) Thermal energy storage density (TESD), and b) Power density (PD) versus dehydration temperature of some salts proposed for SH-TCES. The values represented have been collected from the literature. References are provided in a): $MgCl_2$ and $MgSO_4$ [18], $FeCl_2$ and $CuCl_2$ [22], K_2CO_3 and Na_2S [23], $SrBr_2$ [24].

reducing the effective storage density by > 50 % and increasing overall costs. These factors should be carefully addressed, especially for small-scale applications [13]. On the other hand, liquid-solid hydrations may overcome these limitations and offer advantages in small-scale applications by eliminating the need for an evaporator in closed SH-TCES systems [46]. However, liquid-solid hydration has received limited attention thus far. This study explores a promising SH-TCES scheme based on the direct hydration/dehydration of sodium acetate (SA) with liquid water. Unlike previously proposed salt hydrates, SA allows charging at temperatures suitable for domestic heating applications (30–45 °C) and exhibits rapid liquid-hydration kinetics, greatly enhancing the power density (PD). Furthermore, SA is inexpensive, non-toxic, and abundant [47]. Previous research on SA for energy storage applications has mainly focused on utilizing its solid-liquid phase transition as a latent heat storage material [48–51] or its supercooling capacity for long-term heat storage as a supercooled liquid [47,52]. However, no previous study has provided insights into its reversible hydration/dehydration capacity for thermochemical heat storage at operating temperatures suitable for heating applications.

2. Experimental

2.1. Materials

The sodium acetate trihydrate (SAT, CAS number: 6131-90-4) utilized in this work (> 99.0 %) was supplied by VWR Chemicals. Anhydrous sodium acetate (SA, CAS number: 127-09-3) was obtained by dehydrating in air at 120 °C in a muffle furnace.

For the preparation of SA/silica composites, 1 g of SA was dissolved in a jar containing 5 ml of water, and hydrophile silica (CAS number: 14808-60-7) with a specific BET surface area (SBET) of (200 ± 50) m^2/g (Aerosil TT 600) supplied by evonik operations GmbH. Hydrophile silica was added in different proportions: 5 %, 10 %, and 20 % relative to the mass of SA. Further details regarding the characteristics of the silica used can be found in [53]. Subsequently, the jar was placed on a hot plate to evaporate the water at 50 °C, with air flowing at a rate of 200 ml/min. The mixture was continuously stirred with a magnetic stirrer during the evaporation process. Once dry, the sample consisting of a mixture SA/silica was manually ground in a porcelain mortar to obtain a fine powder.

2.2. Methods

The dehydration process in air was studied from isothermal experiments conducted using a thermogravimetric analyser (TGA) Q5500 IR from TA Instruments. The dehydration of SAT and SAT/silica composites was performed at various temperatures: 30, 40 and 45 °C, with a dry air flow rate of 200 ml/min in a platinum crucible (100 µl, 1 cm in diameter).

The dehydration process in the presence of water vapour (1 % H_2O in air) was studied under isothermal conditions at 35 °C utilizing a thermogravimetric analyser (TGA) Q650 from TA Instruments, in a cylindrical alumina crucible (6.5 mm in diameter and 4 mm in height). Apart from the two standard gas inlets (balance and sample), this instrument is equipped with a third one that was used for injecting air with a steam content of 1 % by volume nearby the sample. The sample size used in the dehydration experiments was 10 mg.

X-ray diffractograms of partially dehydrated SAT were obtained using a Rigaku Miniflex diffractometer, operating at 40 kV and 15 mA, within the 2θ range of 5° to 45°.

2.2.1. Experimental setup for thermochemical performance assessment

Fig. 2a shows a schematic of the experimental setup employed to assess the multicycle performance of SA as a material for TCES by calorimetric measurements. SA and SA/silica composites were placed in a closed glass reactor (with a capacity of 5 ml) that was placed inside a larger glass (with a capacity of 20 ml) jar filled with 2 ml of water. A syringe allows adding water directly to the SA to trigger the hydration reaction. The entire system was thermally insulated with expanded polystyrene to avoid heat losses. Finally, the evolution of temperature is

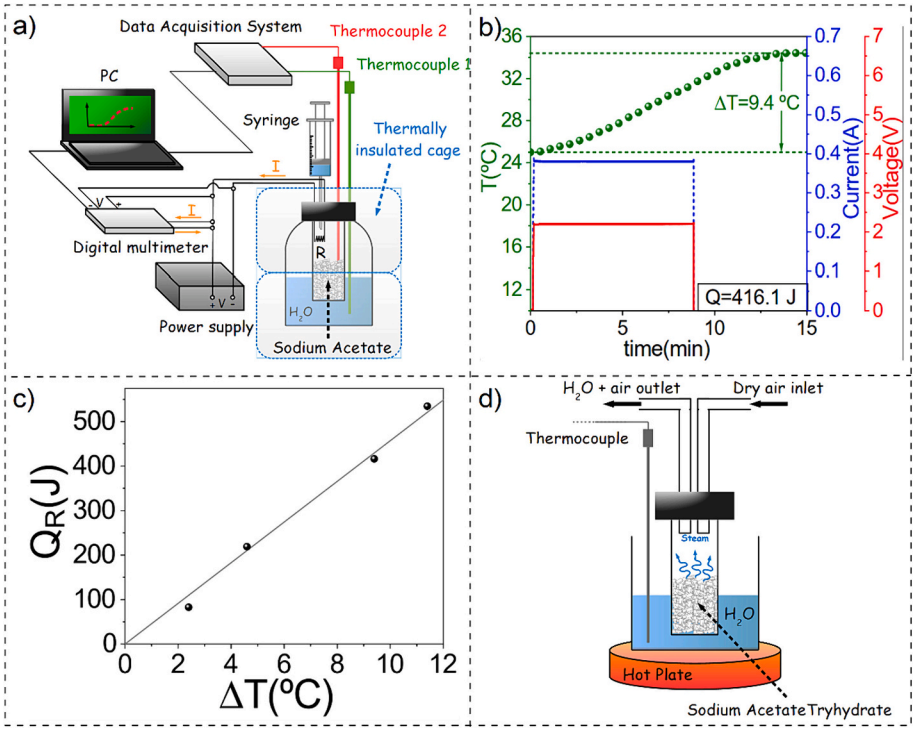

Fig. 2. a) Scheme of the experimental setup used for hydration assessment. b) Fig. 2b shows the voltage and the current imposed together with the time evolution of temperature of water measured with the thermocouple. c) Q_R as a function of ΔT in the experiments conducted to calibrate the system. d) Setup used to carry out the dehydration step.

monitored through two thermocouples; thermocouple 1 was submerged in the water surrounding the reactor, whereas thermocouple 2 was in direct contact with the sample. The readings of the thermocouples were recorded using a data acquisition system connected to a computer (USB-2408-2AO, Measurement Computing), as shown in Fig. 2a.

The setup was calibrated using the dissipated heat of a resistor, inserted in the inner vessel, (R in Fig. 2a) heated by the Joule effect. The energy supplied was calculated from the values of applied current and voltage, which were recorded using a digital multimeter Keithley 2110 5.5. Fig. 2b shows the voltage and the current imposed together with the time evolution of the temperature of water measured with the thermocouple 1. Assuming a linear relationship between the increase in temperature (ΔT) and the heat dissipated in the resistor (Q_R), the heat capacity of the system was determined as the slope of the best-fitting line to the plot Q_R versus ΔT (Fig. 2c):

$$Q_R = C{\cdot}\Delta T \text{ with } C = (45.7 \pm 1.2)\text{J}{\cdot}\text{C}^{-1} \quad (1)$$

2.2.2. Optimization of the experimental setup for determining the SA hydration performance

The hydration of the SA was triggered by adding liquid water with a syringe, as described in Fig. 2. Fig. 3 illustrates, as an example, the readings of the two thermocouples during a hydration experiment performed by adding 0.5 ml of water to 1 g of SA. When the liquid is injected at $t = 0$ min, the sample immediately releases heat, and the thermocouple 2, in contact with the sample, responds accordingly. The maximum temperature is attained in less than one minute (point 1). At the same time, heat is transferred to the rest of the system, and the reading of thermocouple 1 (temperature of the water surrounding the inner vessel) starts rising. The timeframe considered for the test corresponds to the situation when the reading of both thermocouples coincided. At that time (point 2), it is assumed that the system has reached thermal equilibrium. The experiments started at room temperature (25 °C). Thus, the energy released during hydration can be calculated from the increase in temperature observed through Eq. (1). As an example, an increase in temperature of $\Delta T = 8$ °C implies that the energy released is $Q_R = 0.366$ kJ.

At the bottom of Fig. 3, it is shown a sequence of the hydration process (from a top view) recorded with a thermographic camera (PI 1 M, Optris GmbH, Germany). It was recorded with the jar open, adding 1 ml of water to 2 g of SA. Consistently with the measurements of the thermocouples, the sequence illustrates that the heat releases very quickly, reaching a thermal jump of 15.6 °C in < 1 min.

In order to optimize the performance of the system, a series of experiments were conducted by adding varying amounts of water to a fixed quantity of sodium acetate (SA). The observed energy released is plotted in Fig. 4a as a function of the amount of added water, and compared with the expected theoretical values. The variable s represents the ratio of the amount of added water to the stoichiometric value. Thus, for 1 g of SA, $s = 1$ means that the amount added is 0.67 g of water. Q_R has been calculated through Eq. (1) from the temperature rise. Each point in Fig. 4a represents the average of three different measurements. The solid line corresponds to the energy that would be theoretically produced provided all added water reacts with SA to produce SAT. As can be observed, the agreement between experimental data and the theoretical values is good for $s < 0.8$, while a deviation occurs as s goes over that value. This can be ascribed to three effects. Firstly, for values of s above 0.8, part of the added water does not actually react with SA, so not all the potential heat is released. Furthermore, a significant proportion of the heat produced in the reaction is invested in heating the unreacted water. Thirdly, the dissolution of part of SAT in excess water might occur, which is an endothermic process (19.66 kJ·mol^{-1}) [54], and would also absorb part of the energy released during the hydration. The two situations that might occur depending on the values of s are schematised in Fig. 4b. The points in Fig. 4a and the cases illustrated in Fig. 4b share the same background colour. As illustrated on the left in Fig. 4b, since the volume of water is smaller than the volume of SA for small values of s, all the added liquid reacts with SA to form SAT.

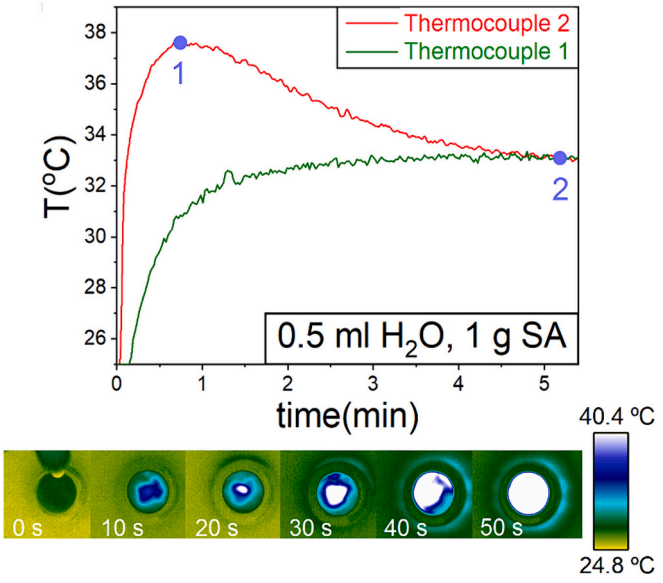

Fig. 3. Example of temperature evolution, measured with both thermocouples, during the hydration. At the bottom, there is a sequence of the process recorded with a thermographic camera.

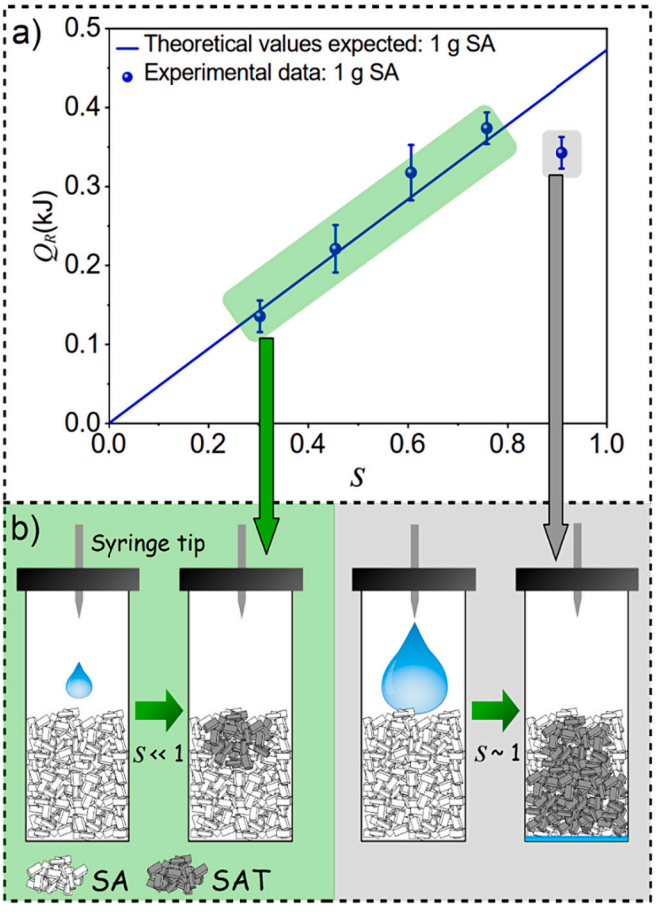

Fig. 4. a) Heat released as a function of the amount of water added at 1 g SA. b) A schematic explanation for the discrepancy between the values of Q_R measured, and the value expected as s increases.

2.2.3. Multicycle hydration/dehydration performance

The experimental setup depicted in Fig. 2a was employed to evaluate the TESD and the PD achievable along a number successive hydration/dehydration tests. As previously described, hydration was conducted by adding water with a syringe directly to the SA. According to the results of the optimization procedure described in the previous section, 0.5 ml of water ($s = 0.75$) were employed in each hydration. Such value was decided from the results in Fig. 4, as it ensures that all the added liquid reacts with SA to form SAT, and no energy is invested in heating the excess water or dissolving SAT.

After hydration, the charging stage was carried out using the setup illustrated in Fig. 2d. The jar containing partially hydrated SA was placed in a hot bath (40 °C) with air flowing at 200 ml/min to carry out dehydration. In this stage, the temperature was also monitored with a thermocouple to ensure dehydration was carried out under isothermal conditions.

3. Results and discussion

The SH-TCES system presented here is based on the following reversible dehydration/hydration reaction:

$$CH_3COONa{\cdot}3H_2O \rightleftharpoons 3H_2O + CH_3COONa, \quad (2)$$

where the enthalpy of the reaction is 39.56 kJ·mol^{-1} [55]. The idea consists of leveraging a renewable source of energy, such as solar power, to drive the endothermic decomposition of SAT. Afterwards, the reaction products, namely water and SA, are stored separately to later combine them and produce the hydration of SA whenever power is needed. The next sections comprise a study of the hydration of SA and multicycle performance in order to assess the feasibility of the proposed TCES system.

3.1. Study of the dehydration process by TGA

In order to determine the SA/SAT system would allow charging at temperatures suitable for domestic heating applications, a series of isothermal experiments were conducted at different temperatures in a TGA. Fig. 5a shows the isothermal dehydration of SAT, carried out at 30, 40 and 45 °C. Table 1 collects the time interval needed for attaining certain degree of dehydration in the conditions explored. As observed, the dehydration rate with dry air is sufficiently high to ensure completion (charge) within ~ 30 min at 45 °C, and approximately in one hour at 30 °C, which is nearly room temperature. The low dehydration temperature exhibited by SAT constitutes an important advantage over other salts proposed for SH-TCES, which typically require dehydration temperatures above 60 °C, falling outside the ideal range for heating applications [12,16].

Fig. 5b displays the results recorded in an experiment conducted in air at 35 °C with 1 % steam by volume of air (partial pressure of 0.01 atm). To provide context, 1 % H_2O by volume of air corresponds to the amount of water in an atmosphere at 15 °C with 65 % relative humidity. This result shows the material could even be fully dehydrated in the presence of humidity in a feasible timescale, with a charging time of approximately two 2 h at the aforementioned conditions. Thus, the possibility of dehydrating SAT with humid air opens up new opportunities for the use of this material in SH-TCES open systems [16,46].

The X-ray diffractogram of a sample of SAT partially dehydrated is shown in Fig. 5c. Before conducting the X-ray measurement, the sample underwent partial dehydration in dry air using the experimental setup depicted in Fig. 2d. At the time of measurement, 30 % degree of the starting SAT had undergone dehydration. The pattern observed can be indexed with monoclinic sodium carbonate trihydrate (00–028-1030) and orthorhombic anhydrous sodium acetate (00–029-1158), which indicates that the presence of intermediates with different degrees of hydration can be discarded.

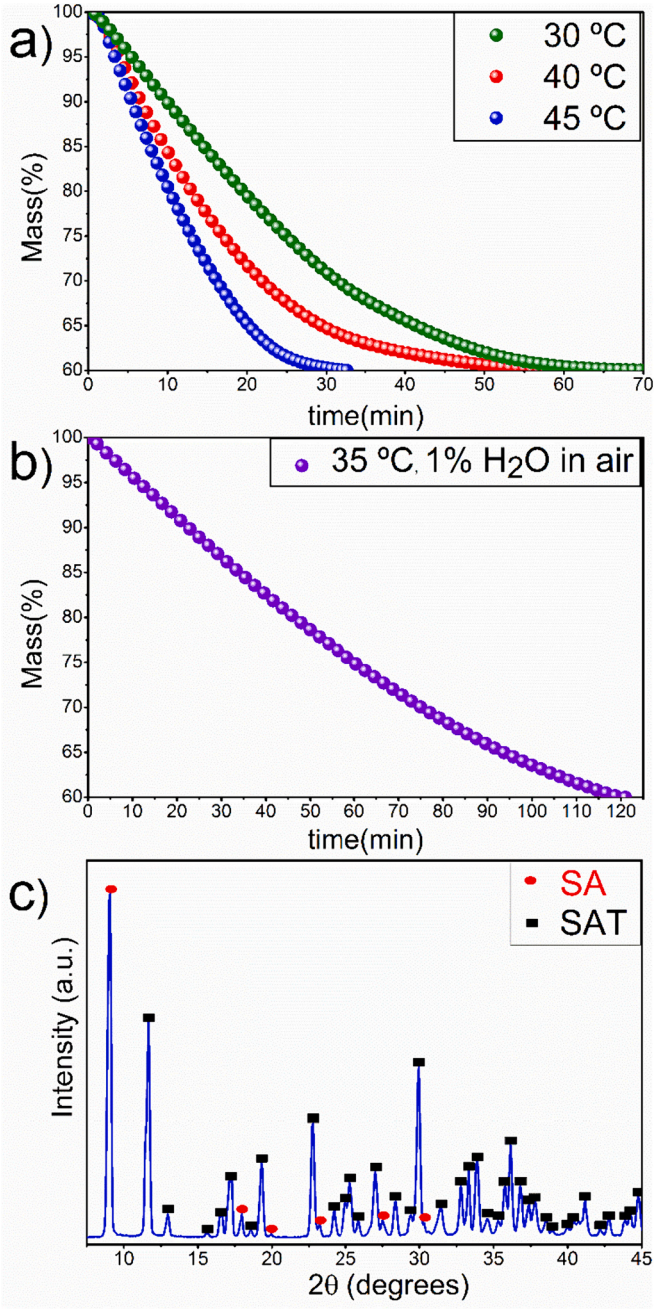

Fig. 5. a) Isothermal dehydration of SAT at different temperatures: 30, 40 and 45 °C. b) Isothermal dehydration of SAT at 35 °C with and without steam (1 % by volume). c) X-ray diffractogram of partially dehydrated SAT.

Table 1
Time interval (minutes) needed for attaining 50, 75 and 100 % charge in the conditions explored.

Conditions	Charge level		
	50 %	75 %	100 %
30 °C, dry air	19.5 min	31.5 min	65 min
40 °C, dry air	13 min	22 min	54 min
45 °C, dry air	10 min	16 min	32.5 min
35 °C, 1 % H_2O (g) in air	46 min	75 min	121 min

3.2. Multicycle performance of a sodium acetate-based SH-TCES system

This section evaluates the SAT-based SH-TCES system along a number of ensuing hydration and dehydration cycles, in order to assess its multicycle performance. The experiments were performed as detailed in the Experimental section. Fig. 6 shows the degree of conversion X_N attained, the energy per mass unit, and the power density attained during the hydration stage in the multicycle tests. The parameter X_N is defined as the ratio of the energy released in the hydration stage $Q_{R,N}$, and the expected when 1 g of SA completely reacts with the stoichiometric amount of water to form SAT. The amount of water that would be required for full conversion is ~ 0.67 ml, which corresponds to a released heat of 477 J. Thus, X_N is calculated according to the following equation:

$$X_N = \frac{Q_{R,N}(J)}{477} \quad (3)$$

The multicycle performances of SA regenerated by flowing air to promote dehydration is depicted in Fig. 6a and b. The tests were conducted using 1 g SA and 0.5 ml of liquid water (s = 0.75). The PD has been estimated as the ratio between the energy density and the time needed to attain the maximum temperature value when water is injected, which as observed in Fig. 3, is approximately 60 s.

As may be observed, the conversion drops with the cycle number. It is well-known that the deliquescent character of salt hydrates leads to particle aggregation, which is one of the main causes of the deactivation of hydration [21,34,38]. Fig. 7a shows a picture of the sorbent before the multicycle tests and after 10 cycles, where the aggregation is clear.

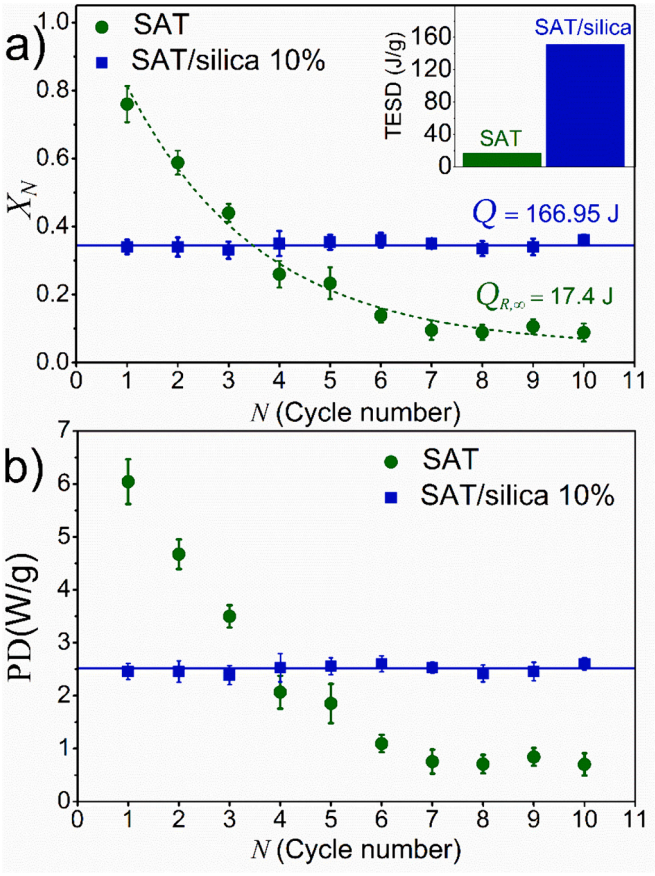

Fig. 6. Multicycle performance of SA regenerated by dehydration in air, and the mixture 10 % silica/SA. The best fitting to Eq. (S5) (see the supplementary data section) is represented with a dashed green line. b) Power density as a function of the cycle number. (For interpretation of the references to colour in this figure legend, the reader is referred to the web version of this article.)

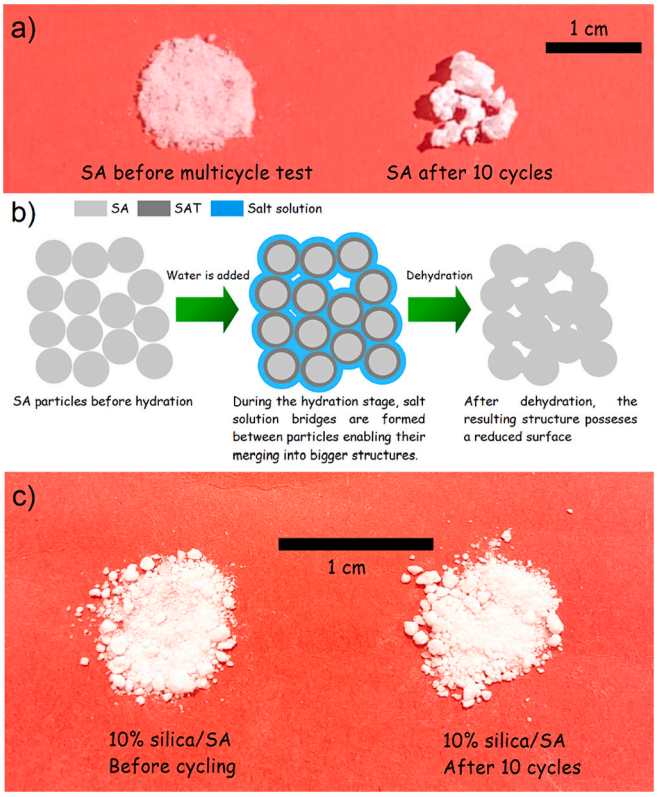

Fig. 7. a) Picture of the sample before and after the multicycle test. b) Illustration of the deactivation process undergone by the SA sorbent after cycling. c) Picture of the sample with 10 % silica content before and after the multicycle test.

Fig. 7b illustrates the deactivation process. The solid-liquid reaction considered here occurs mainly on the surface of the SA particles, and as with any other deliquescent salt, SA dissolves in water. Thus, the water added reacts with SA to form SAT while concomitantly serving as a solvent for SA. The liquid solution creates bridges between the particles, promoting their merging to form SA aggregates after drying, reducing the solid surface area for reacting with water in the next cycle. This deactivation will continue during the cycles until a minimum surface is reached. Since the material is expected to be cycled many times in real applications, it is important to provide the value of the residual conversion, which is the conversion attained after a large number of cycles. To this end a semiempirical model has been derived, which complete description can be found in the supplementary data section. Experimental data in Fig. 6 can be fitted by Eq. (S5) (see the supplementary data section) by selecting the proper parameters. The best-fitting line has been plotted in Fig. 6 as a green dashed line. The fitting is reasonably good and provides a value for the residual conversion of ~0.04 (equivalently $Q_{R,\infty}$= 17.4 J). Such value would correspond to a PD of about 0.5 W/g.

The deactivation phenomena observed could be prevented by a soft manual disaggregation of the material after each discharging stage. In this later case, conversion and power density remain constant with the cycle number, at an average value of $\overline{X} = 0.75 \pm 0.05$. It is worth noticing that SA exhibits low mechanical resistance to disaggregation. Indeed, in our experiments, the material was easily disaggregated by hand using a plastic spatula, recovering its appearance before hydration (as shown in Fig. 7a left). However, integrating a mechanical setup within the SH-TCES system to disaggregate and regenerate the sorbent after hydration would be necessary, which might also entail technical difficulties.

Considering that mechanical disaggregation limits the applicability

of the proposed SH-TCES system, it would be worthwhile to investigate alternative solutions. In this regard, previous studies on different systems have proposed the impregnation of silica-gel matrices for successfully improving the cyclability of salts hydrates (SH-TCES systems) [52,56]. Silica gel is a mesoporous desiccant attractive for TCES because of its affordability (~ 30 € per kg), high specific surface area (approximately 10^2–10^3 m^2/g), proper charging temperature and non-toxicity [57].

Motivated by these studies, the multicycle performance of silica/SA composites with different silica content was tested in the same conditions as pure SA. Fig. 6a and b show the multicycle performance of the composite containing a mixture of 10 % silica/SA in mass. The composite exhibited a stable conversion during the 10 cycles with a thermal energy storage density of 151.8 J/g and a power density of 2.52 W/g (approximately 35 % of the maximum value theoretically achievable), without needing a mechanical system to regenerate the sorbent. The TESD values attained with pure SA and the composite are compared in the inset in Fig. 6a. Notice that while the experiment involving pure SA utilized 1 g of material and the TESD can be estimated as $Q_{R,\infty}/1g$ = 17.4 J/g, the test conducted with the composite containing 10 % silica required 1.1 g in order to compare the results with pure SA and the TESD value needs to be calculated as 166.95 J/1.1g = 151.8 J/g. Therefore, 10 % silica increases the thermal energy storage density from 17.4 J/g to 151.8 J/g. Fig. 7c shows pictures of the samples before and after 10 cycles. The sample preserved its appearance, and aggregation was not observed.

The positive effect of silica to stabilise the multicycle performance of the sorbent can be explained in terms of its hydrophile character. Thus, on the one hand, hydrophilic silica absorbs parts of the water added during the hydration stage, attenuating the deliquescence. On the other hand, the presence of silica reduces the contact between SA particles, preventing aggregation and loss of reactive area.

Table 2 collects the average conversion and TESD values attained in 10 cycles with its standard deviations for SA samples with different silica content (5 %, 10 % and 20 % in mass relative to the mass of SA). As might be observed, the results are similar for the three composites tested, with a slight decrease for the sample with the highest content in silica. For comparison, the TESD and conversion values obtained for pure SA are also collected in Table 2. For SA dehydrated without disaggregation, the value of conversion provided in Table 2 corresponds to the residual conversion calculated as $X_\infty = Q_{R,\infty}/477$.

The energy density of sensible heat storage in water has been included in Table 2 for comparison. This reference magnitude in water has been calculated according to the thermal energy required to increase the temperature of water by 25 °C (e.g. from 25 to 30 °C to 50–55 °C), which is the typical increase expected for domestic heating applications. Remarkably, the 10 % silica/SA have a TESD 50 % higher than water under the boundary conditions required in heating applications.

The comparison between SA and other TCMs indicates that it possesses lower TESD. For instance, theoretically TESD of SA is 480 J/g, while $CuCl_2$, as shown in Fig. 1a has a TESD of 520 J/g. Still, the PD theoretically achievable (~8 W/g) is nearly two orders of magnitude higher than those reported in previous studies (~0.1 W/g, see Fig. 1b). This high value of thermal heating capacity, much higher than those previously observed in steam-based reactions of salts [12,16], would facilitate the integration of thermal batteries for heating supply. The proposed TCES system exhibit the capability to respond quickly to heating demand without heat pump operation.

4. Conclusions

This study analyses a promising thermochemical energy storage system based on the hydration/dehydration of sodium acetate with liquid water. Based on the results obtained here, the following conclusions are drawn:

Contrary to what happens with most storage systems previously studied, the SA-based system proposed here can be fully charged at temperatures within the range suitable for domestic heating applications (40 °C-60 °C).

The system attains up to 75 % (357.8 J/g) of the theoretical energy storage capability in the first cycle and this value decreases with the cycle number due to aggregation, which only could be prevented by a soft mechanical treatment. Since this disaggregation process limits the applicability of the proposed SH-TCES system, a silica/SA composite has been prepared and tested under the same conditions of pure SA. It is demonstrated that 10 % silica addition helps preventing the sorbent deactivation without any mechanical interaction, achieving a stable conversion rate of 35 % (151.8 J/g) of the theoretical storage capability.

The SA-based system stands for its power density. While the hydration power density of other salts (hydrated in steam) ranges between 0.1 and 0.25 W/g, hydration with liquid water produces an almost instantaneous heat release that reflects in a much higher power density (5.96 W/g) and eases the integration of heat into the electricity grid.

Summarising, this study highlights the potential use of sodium acetate for thermochemical energy storage in heating applications. The studied system presents low hydration and dehydration temperatures adequate for heating applications, and with power density values nearly two orders of magnitude higher than the previously reported for other salts. Additionally, it should be highlighted the potential dual/hybrid TES performance offered by this material to store thermal energy through a thermochemical energy storage process such as the one proposed here or a more conventional latent heat process.

Table 2
Average ($\overline{X}$) and residual conversion (X_∞) attained by the samples studied along with thermal energy storage density (TESD). The thermal energy density attained with sensible heat storage in water is provided for comparison.

Sample	X_∞	$\overline{X}$	*TESD* (J/g)
SA (dehydration in air + hydration)	0.036 ± 0.005	–	17.4
SA (dehydration in air + disaggregation + hydration)	–	0.75 ± 0.05	357.8
5 % silica/SA (dehydration in air + hydration)	–	0.32 ± 0.02	145.4
10 % silica/SA (dehydration in air + hydration)	–	0.35 ± 0.01	151.8
20 % silica/SA (dehydration in air + hydration)	–	0.30 ± 0.02	119.3
Sensible heat storage in water	–	–	104.5

Author's statement

The experimental data used to prepare this publication will be available on request to any researchers interested in them.

CRediT authorship contribution statement

Juan Arcenegui-Troya: Data curation, Formal analysis, Investigation, Writing – original draft. **Jesus Lizana:** Conceptualization, Writing – original draft. **Pedro Enrique Sánchez-Jiménez:** Project administration, Supervision, Writing – review & editing. **Antonio Perejón:** Conceptualization, Methodology, Supervision. **Andrea Vañes-Vallejo:** Investigation. **Luis Allan Pérez-Maqueda:** Funding acquisition, Project administration, Resources, Supervision.

Declaration of competing interest

The authors declare that they have no known competing financial interests or personal relationships that could have appeared to influence the work reported in this paper.

Data availability

Data will be made available on request.

Acknowledgements

This work was supported by MCIN/AEI/10.13039/501100011033 and European Union Next Generation EU/PRTR (Nos. PDC2021-121552-C21 and PID2022-140815OB-C22) and Ministerio de Ciencia e Innovación (No. TED2021-131839B-C22).

Appendix A. Supplementary data

Supplementary data to this article can be found online at https://doi.org/10.1016/j.est.2024.111310.

References

[1] IEA. Energy & CO2 status report, Available from, https://www.iea.org/reports/global-energy-CO2-status-report-2019, 2019. (Accessed 18 August 2021).
[2] Irena, Innovation Outlook: Thermal Energy Storage, 2020, p. 144.
[3] J. Lizana, et al., A national data-based energy modelling to identify optimal heat storage capacity to support heating electrification, Energy 262 (2023) 125298.
[4] R. Gross, R. Hanna, Path dependency in provision of domestic heating, Nat. Energy 4 (5) (2019) 358–364.
[5] S.K. Shah, L. Aye, B. Rismanchi, Seasonal thermal energy storage system for cold climate zones: a review of recent developments, Renew. Sustain. Energy Rev. 97 (2018) 38–49.
[6] K. Du, et al., A state-of-the-art review of the application of Phase Change Materials (PCM) in Mobilized-Thermal Energy Storage (M-TES) for recovering low-temperature Industrial Waste Heat (IWH) for distributed heat supply, Renew. Energy 168 (2021) 1040–1057.
[7] L.F. Cabeza, et al., Perspectives on thermal energy storage research, Energy 231 (2021) 120943.
[8] A. Santos, F. Almeida, F. Neto, Development of rock sensible heat storage system: modeling of a hematite reservoir, J. Energy Storage 40 (2021) 102818.
[9] S. Lu, et al., Study on thermal performance improvement technology of latent heat thermal energy storage for building heating, Appl. Energy 323 (2022) 119594.
[10] G. Airò Farulla, et al., A review of thermochemical energy storage systems for power grid support, Appl. Sci. 10 (9) (2020).
[11] F. Desai, et al., Thermochemical energy storage system for cooling and process heating applications: a review, Energy Convers. Manag. 229 (2021) 113617.
[12] P.A.J. Donkers, et al., A review of salt hydrates for seasonal heat storage in domestic applications, Appl. Energy 199 (2017) 45–68.
[13] J. Lizana, et al., Advanced low-carbon energy measures based on thermal energy storage in buildings: a review, Renew. Sustain. Energy Rev. 82 (2018) 3705–3749.
[14] W. Hua, et al., Review of salt hydrates-based thermochemical adsorption thermal storage technologies, J. Energy Storage 56 (2022) 106158.
[15] A. Fopah Lele, et al., Thermal decomposition kinetic of salt hydrates for heat storage systems, Appl. Energy 154 (2015) 447–458.
[16] W. Li, et al., Salt hydrate–based gas-solid thermochemical energy storage: current progress, challenges, and perspectives, Renew. Sustain. Energy Rev. 154 (2022) 111846.
[17] L. Okhrimenko, et al., Thermodynamic study of MgSO4 – H2O system dehydration at low pressure in view of heat storage, Thermochim. Acta 656 (2017) 135–143.
[18] C.J. Ferchaud, et al., Study of the reversible water vapour sorption process of $MgSO_4.7H_2O$ and $MgCl_2.6H_2O$ under the conditions of seasonal solar heat storage, J. Phys. Conf. Ser. 395 (2012) 012069.
[19] M. Gaeini, S.A. Shaik, C.C.M. Rindt, Characterization of potassium carbonate salt hydrate for thermochemical energy storage in buildings, Energ. Buildings 196 (2019) 178–193.
[20] L.-C. Sögütoglu, et al., Understanding the hydration process of salts: the impact of a nucleation barrier, Cryst. Growth Des. 19 (4) (2019) 2279–2288.
[21] A. Fopah-Lele, J.G. Tamba, A review on the use of SrBr2·6H2O as a potential material for low temperature energy storage systems and building applications, Sol. Energy Mater. Sol. Cells 164 (2017) 175–187.
[22] L. Glasser, Thermodynamics of inorganic hydration and of humidity control, with an extensive database of salt hydrate pairs, J. Chem. Eng. Data 59 (2) (2014) 526–530.
[23] L.C. Sögütoglu, et al., In-depth investigation of thermochemical performance in a heat battery: cyclic analysis of K2CO3, MgCl2 and Na2S, Appl. Energy 215 (2018) 159–173.
[24] J. Stengler, I. Bürger, M. Linder, Thermodynamic and kinetic investigations of the SrBr2 hydration and dehydration reactions for thermochemical energy storage and heat transformation, Appl. Energy 277 (2020) 115432.
[25] N. Mazur, et al., Impact of polymeric stabilisers on the reaction kinetics of SrBr2, Sol. Energy Mater. Sol. Cells 238 (2022) 111648.
[26] S. Wei, et al., Influence of minerals with different porous structures on thermochemical heat storage performance of CaCl2-based composite sorbents, Sol. Energy Mater. Sol. Cells 243 (2022) 111769.
[27] M.A.R. Blijlevens, et al., A study of the hydration and dehydration transitions of SrCl2 hydrates for use in heat storage, Sol. Energy Mater. Sol. Cells 242 (2022) 111770.
[28] J. Lizana, et al., Identification of best available thermal energy storage compounds for low-to-moderate temperature storage applications in buildings, Mater. Constr. 68 (331) (2018) 1–35.
[29] E. Osterman, U. Stritih, Review on compression heat pump systems with thermal energy storage for heating and cooling of buildings, J. Energy Storage 39 (2021) 102569.
[30] D. Mohapatra, J. Nandanavanam, Salt in Matrix for Thermochemical Energy Storage - a Review, in: Materials Today: Proceedings, 2022.
[31] G. Whiting, et al., Heats of water sorption studies on zeolite–MgSO4 composites as potential thermochemical heat storage materials, Sol. Energy Mater. Sol. Cells 112 (2013) 112–119.
[32] Q. Wang, et al., Structure and hydration state characterizations of MgSO4-zeolite 13x composite materials for long-term thermochemical heat storage, Sol. Energy Mater. Sol. Cells 200 (2019) 110047.
[33] Q. Touloumet, et al., Investigation of the impact of zeolite shaping and salt deposition on the characteristics and performance of composite thermochemical heat storage systems, J. Mater. Chem. A 11 (6) (2023) 2737–2753.
[34] Y.N. Zhang, et al., Development and thermochemical characterizations of vermiculite/SrBr2 composite sorbents for low-temperature heat storage, Energy 115 (2016) 120–128.
[35] A.I. Shkatulov, et al., Stabilization of K2CO3 in vermiculite for thermochemical energy storage, Renew. Energy 150 (2020) 990–1000.
[36] Z. Chen, et al., A study on vermiculite-based salt mixture composite materials for low-grade thermochemical adsorption heat storage, Energy 278 (2023) 127986.
[37] A. Cammarata, et al., Hybrid strontium bromide-natural graphite composites for low to medium temperature thermochemical energy storage: formulation, fabrication and performance investigation, Energy Convers. Manag. 166 (2018) 233–240.
[38] S. Salviati, et al., Ice-templated nanocellulose porous structure enhances thermochemical storage kinetics in hydrated salt/graphite composites, Renew. Energy 160 (2020) 698–706.
[39] W. Shi, et al., Water sorption properties of functionalized MIL-101(Cr)-X (X=-NH2, –SO3H, H, –CH3, –F) based composites as thermochemical heat storage materials, Microporous Mesoporous Mater. 285 (2019) 129–136.
[40] H. Yang, et al., Salt hydrate adsorption material-based thermochemical energy storage for space heating application: a review, Energies 16 (2023), https://doi.org/10.3390/en16062875.
[41] H.U. Rammelberg, et al., Thermochemical heat storage materials – performance of mixed salt hydrates, Sol. Energy 136 (2016) 571–589.
[42] ASHRAE, Handbook - Fundamentals, SI Edition edn, 2017.
[43] B. Longuet, P. Gillard, Experimental investigation on the heterogeneous kinetic process of the low thermal decomposition of ammonium perchlorate particles, Propellants Explos. Pyrotech. 34 (1) (2009) 59–71.
[44] J. Jung, et al., A new reactor for the analysis of thermal decomposition reactions, Thermochim. Acta 55 (2) (1982) 161–172.
[45] N. Kameno, N. Koga, Heterogeneous kinetic features of the overlapping thermal dehydration and melting of thermal energy storage material: sodium thiosulfate pentahydrate, J. Phys. Chem. C 122 (15) (2018) 8480–8490.
[46] Z.Y. Zeng, B.C. Zhao, R.Z. Wang, Passive day and night heating for zero energy buildings with solar-based adsorption thermal battery, Cell Rep. Phys. Sci. 2 (9) (2021) 100578.
[47] J. Lizana, et al., Supercooled sodium acetate aqueous solution for long-term heat storage to support heating decarbonisation, J. Energy Storage 55 (2022) 105584.
[48] M. Kenisarin, K. Mahkamov, Salt hydrates as latent heat storage materials: Thermophysical properties and costs, Sol. Energy Mater. Sol. Cells 145 (2) (2016) 255–286.
[49] N. Xie, et al., Salt hydrate/expanded vermiculite composite as a form-stable phase change material for building energy storage, Sol. Energy Mater. Sol. Cells 189 (July 2018) (2019) 33–42.
[50] K. Yu, Y. Liu, Y. Yang, Review on form-stable inorganic hydrated salt phase change materials: preparation, characterization and effect on the thermophysical properties, Appl. Energy 292 (2021) 116845.
[51] L.F. Cabeza, et al., Thermal performance of sodium acetate trihydrate thickened with different materials as phase change energy storage material, Appl. Therm. Eng. 23 (13) (2003) 1697–1704.
[52] E. Courbon, et al., Further improvement of the synthesis of silica gel and CaCl2 composites: enhancement of energy storage density and stability over cycles for solar heat storage coupled with space heating applications, Sol. Energy 157 (2017) 532–541.
[53] EVONIK, Permanently resilient: AEROSIL® fumed silica from EVONIK for adhesives and sealants, Available from: https://www.silica-specialist.com/en/our-markets/adhesives-and-sealants, 2023. (Accessed 20 June 2023).
[54] W.M. Haynes, D.R. Lide, T.J. Bruno (Eds.), CRC Handbook of Chemistry and Physics, 97th ed., 2016.
[55] S.K. Sharma, C.K. Jotshi, S. Kumar, Kinetics of dehydration of sodium salt hydrates, Thermochim. Acta 184 (1) (1991) 9–23.
[56] P. D'Ans, et al., Humidity dependence of transport properties of composite materials used for thermochemical heat storage and thermal transformer appliances, J. Energy Storage 18 (2018) 160–170.
[57] R. Erlund, R. Zevenhoven, Thermal Energy Storage (TES) capacity of a lab scale magnesium hydro carbonates/silica gel system, J. Energy Storage 25 (2019) 100907.